PROCEEDINGS, Twenty-Sixth Workshop on Geothermal Reservoir Engineering
Stanford University, Stanford, California, January 29-31, 2001
SGP-TR-168

NEW ANALYTICAL MODELS FOR THE GROWTH OF THE THERMAL ZONE IN FRACTURED GEOETHERMAL RESERVOIRS

John C. Reis

Embry-Riddle University
3200 Willow Creek Road
Prescott, AZ 86301 USA
reis@pr.erau.edu

ABSTRACT

This paper presents new analytical models for predicting the areal extent of the thermal zone in a fractured geothermal reservoir during reinjection. Models for the early- and late-time conduction periods are presented, as are models for both double- and triple-porosity reservoirs. Methods for incorporating measured fracture spacing distribution data (instead of assuming uniform-sized matrix blocks) are also presented.

INTRODUCTION

A variety of analytical models have been developed for predicting the convective flow of heat through geothermal reservoirs during reinjection (Lauwerier, 1955; Gringarten et al., 1975; Bodvarsson and Tsang, 1982; Satman, 1988; Marx and Langenheim, 1959; Hearn, 1969; Closmann, 1967). While these models have been useful, they all have limitations. These limitations include models limited to one-dimension, models applicable only during the early-time period when conduction in the matrix block is as if into a semi-infinite medium, models that are too complex for practical use, and models that have analytical solutions only in the Laplace domain. In this paper, new analytical models for the advance of thermal fronts in geothermal reservoirs are developed that overcome many of these limitations. These new thermal advance models use matrix conduction models that were previously presented (Reis, 2000).

THERMAL ADVANCE IN FRACTURE NETWORKS

The areal extent of the thermal zone is obtained by applying an energy balance to the injected water. For the case of the fracture porosity (as a function of bulk formation volume) being negligible, i.e., the fluid in the fractures have a negligible thermal capacity, this energy balance can be written as

$$q_{w,inj} = \int_0^t q_{A,1}(t-\tau)\,\frac{dA}{d\tau}\,d\tau + \int_0^t q_{A,2}(t-\tau)\,\frac{dA}{d\tau}\,d\tau, \qquad (1)$$

where $q_{w,inj}$ is the enthalpy of the injected water, the integrals are the thermal crossflow from the fracture network to two different matrix domains, and A is the surface area of the heated zone as seen from the top of the horizontal formation (not the surface area of the matrix blocks themselves).

Early-Time Period

The early-time period thermal advance models are obtained by using the early-time period conduction model in the energy balance integrals. For the early-time period, i.e., for the case when the conduction fronts from opposing faces within the matrix blocks do not yet reach the center of the matrix blocks, the conduction rate per unit area of the heated zone (as seen from above the formation) can be expressed as (Reis, 2000)

$$q_A = \chi\omega\left[J\sqrt{\frac{t_{cl}}{t}} - K + M\sqrt{\frac{t}{t_{cl}}}\right], \qquad (2)$$

where

$$\omega = \frac{H\rho_m c_m \Delta T}{t_{cl}}, \qquad (3)$$

$$J = \frac{1}{12}\left(1 + \frac{L_x}{L_y} + \frac{L_x}{L_z}\right)\sqrt{\frac{D_L}{\pi}}, \qquad (4)$$

$$K = \frac{1}{36}\left(\frac{L_x}{L_y} + \frac{L_x}{L_z} + \frac{L_x^2}{L_y L_z}\right)\frac{D_L}{\pi}, \qquad (5)$$

$$M = \frac{1}{144}\frac{L_x^2}{L_y L_z}\sqrt{\left(\frac{D_L}{\pi}\right)^3}, \qquad (6)$$

$$D_L = \frac{\left(4L_xL_y + 4L_xL_z + 36L_yL_z - 5L_x^2\right)}{\left(L_xL_y + L_xL_z + L_yL_z\right)}, \quad (7)$$

$$t_{cl} = \frac{L_x^2}{576\alpha} D_L, \quad (8)$$

L_x, L_y, and L_z are the matrix block dimensions, χ is the volume fraction of an individual matrix domain, H is the formation thickness, and α is the thermal diffusivity.

Substituting Eq. 2 into Eq. 1 and solving for the area of the thermal zone yields

$$A(t) = \frac{q_{w,inj}}{E_1}\left[\begin{array}{l} f_1 a \exp\{a^2 t\}\operatorname{erfc}\{a\sqrt{t}\} \\ -f_2 b \exp\{b^2 t\}\operatorname{erfc}\{b\sqrt{t}\} \end{array}\right], \quad (9)$$

where

$$a = \frac{1}{2}\frac{E_2}{E_1} + \frac{\sqrt{\left(\frac{E_2}{E_1}\right)^2 - 4\frac{E_3}{E_1}}}{2}, \quad (10)$$

$$b = \frac{1}{2}\frac{E_2}{E_1} - \frac{\sqrt{\left(\frac{E_2}{E_1}\right)^2 - 4\frac{E_3}{E_1}}}{2}, \quad (11)$$

$$f_1 = \frac{1}{a(b-a)}, \quad (12)$$

$$f_2 = \frac{1}{a(b-a)} - \frac{1}{ab}, \quad (13)$$

$$E_1 = \chi_1\omega_1 J_1\sqrt{\pi t_{cl,1}} + \chi_2\omega_2 J_2\sqrt{\pi t_{cl,2}}, \quad (14)$$

$$E_2 = \chi_1\omega_1 K_1 + \chi_2\omega_2 K_2, \quad (15)$$

and

$$E_3 = \frac{\chi_1\omega_1 M_1}{\sqrt{t_{cl,1}}}\frac{\sqrt{\pi}}{2} + \frac{\chi_2\omega_2 M_2}{\sqrt{t_{cl,2}}}\frac{\sqrt{\pi}}{2}. \quad (16)$$

The subscripts on the right-hand side of these equations refer to the individual matrix block domains. This model has the following restrictions on the matrix block dimensions:

$$L_y \geq L_x \quad (17)$$

and

$$L_z \geq \left[\begin{array}{l} \frac{1}{2}\left(\frac{3\pi}{2} - 2\right)\left(L_x + L_y\right) \\ \pm\frac{1}{2}\sqrt{\left[\left(2 - \frac{3\pi}{2}\right)\left(L_x + L_y\right)\right]^2 - 4\left[\left(2 - \frac{3\pi}{2}\right)L_xL_y + L_y^2 + L_x^2\right]} \end{array}\right]. \quad (18)$$

Late-Time Period

The late-time period thermal advance models are obtained by using the late-time period conduction model in the energy balance integrals. For the late-time period, i.e., for the case when the conduction fronts from opposing faces of the matrix blocks interfere with each other, the conduction rate per unit area of the heated zone can be expressed as (Reis, 2000)

$$q_A = \frac{q}{dA} = \frac{\chi H\rho c\Delta T\delta}{t_{cl}}\exp\left\{-\delta\frac{t}{t_{cl}}\right\}, \quad (19)$$

where

$$\delta = \ln\left[\frac{12L_yL_z}{L_x^2 + 6L_yL_z - 2L_xL_y - 2L_xL_z}\right], \quad (20)$$

ρ and c are the density and heat capacity of the matrix, and ΔT is the difference between the initial formation temperature and injected water temperature. Substituting Eq. 19 into Eq. 1 and solving for the area of the thermal zone yields

$$A(t) = \frac{q_{w,inj}}{H\rho c\Delta T\alpha}\left[\begin{array}{l} \left(\frac{(R_1+R_2) - (\chi_1R_1 + \chi_2R_2)}{R_1R_2}\right) \\ +\alpha t \\ \left(\frac{1}{(\chi_1R_1 + \chi_2R_2)}\right) \\ +\left(-\left(\frac{(R_1+R_2) - (\chi_1R_1 + \chi_2R_2)}{R_2R_1}\right)\right) \\ *\exp\left\{-\frac{R_1R_2}{(\chi_1R_1 + \chi_2R_2)}\alpha t\right\} \end{array}\right], \quad (21)$$

where it has been assumed that the thermal properties of the matrix blocks in the two domains are equal but matrix block sizes are not, i.e., the fractures cut homogeneous rock, and a matrix block size parameter has been defined as

$$R = \frac{576\left(L_xL_y + L_xL_z + L_yL_z\right)\delta}{L_x^2\left(4L_xL_y + 4L_xL_z + 36L_yL_z - 5L_x^2\right)}. \quad (22)$$

This model does not have any restrictions on matrix block dimensions other than the dimensions being ordered such that $L_x < L_y < L_z$.

For the case of a double porosity reservoir, i.e., one matrix domain ($R_1 = R_2$), Eq. 21 simplifies to

$$A(t) = \frac{q_{w,inj}}{H\rho c\Delta T\alpha}\left[\frac{1}{R} + \alpha t\right]. \quad (23)$$

INCORPORATION OF FRACTURE DATA IN NETWORK MODEL

In naturally-fractured formations, fracture properties normally govern fluid flow through the reservoir. In most reservoir models, it is assumed that all fractures are uniformly spaced and all matrix blocks are identical. Fractures, however, are not uniformly

spaced and the utility of this assumption remains largely untested.

Although exact information about the fracture locations, distributions, spacings, and apertures in the reservoir can never be completely known, relevant statistical fracture properties can often be obtained from outcrop and/or wellbore measurements. These statistical fracture properties can then be used in reservoir models to determine the probable reservoir behavior. In this section, methods for incorporating statistical parameters from measured fracture spacing distributions into the models for the area of the thermal zone will be presented. The outcome of this analysis is to determine the appropriate values of L_x, L_y, and L_z to be used in the thermal advance models.

The fracture spacing distribution used in this study is the negative-exponential model (Mahtab et al., 1973; Call et al., 1976; Priest and Hudson, 1976; Baecher et al., 1977; Einstein et al., 1979; Wallis and King, 1980; Einstein and Baecher, 1983; and Sen and Eissa, 1992). Other distributions have been discussed by these and other authors.

Early-Time Period: Single Matrix Domain

Fracture spacing data is incorporated in the single matrix domain, early-time period model by noting that thermal crossflow between the fractures and matrix blocks during this period is controlled by the surface area of the matrix blocks. Many small matrix blocks result in a large matrix block surface area and a rapid energy transfer. The average surface area per matrix block was calculated for a reservoir having a different negative-exponential fracture spacing distribution in each of the three directions using a Monte Carlo approach. Over 10,000 individual matrix blocks were simulated for each assumed set of average fracture spacings. The surface area was calculated for each matrix block and the average of all of the matrix blocks was determined. The average surface area per matrix block was then compared to the corresponding surface area calculated assuming all matrix blocks were identical and had dimensions equal to the average fracture spacing in each respective direction. As seen in Fig. 1, the average matrix block surface area for a reservoir having a negative-exponential fracture spacing distribution is virtually identical to that of a reservoir having uniformly spaced fractures with the same average spacing. Each point in this figure corresponds to a different set of assumed average fracture spacings. This result is to be expected as long as the orthogonal fracture spacings are independent of each other.

Based on this result, the fracture spacing distribution data are incorporated into the one matrix domain, early-time period model by using the average fracture spacings in each direction in Eq. 9. These spacings are ordered such that $L_x < L_y < L_z$. Since there is only one matrix domain, $\chi_1 = 1$ and $\chi_2 = 0$.

Early-Time Period: Two Matrix Domains

The fracture spacing data for two matrix domains is incorporated into the early-time period model by finding an appropriate average matrix block surface area for each matrix domain and then selecting appropriate fracture spacings for each domain that yield the desired average matrix block surface area. One domain will tend to have the smaller matrix blocks and the other will have the larger matrix blocks.

The first step is to select the volume fractions associated with each domain. This is a choice made by the user. Then the midrange cumulative volume fractions for each matrix domain are determined. The midrange volume fraction is the characteristic cumulative volume fraction for each domain. If the matrix domains are assumed to each occupy 50% of the reservoir, the midrange cumulative volume fractions are 25% (midrange between 0 and 50%) and 75% (midrange between 50 and 100%). If the matrix domains are assumed to be 25% and 75% of the reservoir volume, the midrange cumulative volume fractions are 12.5% and 62.5%, respectively.

Next the surface area for matrix blocks in each domain is obtained from the midrange volume fraction. A relationship between the matrix block volume and surface area was obtained through a Monte Carlo analysis. For a particular set of average fracture spacings in three orthogonal directions, thousands of realizations of specific fracture spacings were generated and the surface area and volume of each corresponding matrix block was calculated. These data were then sorted by increasing matrix block volume. The cumulative surface area was then calculated as a function of cumulative matrix block volume for the entire set of matrix blocks realizations. These curves were normalized by the total surface area and volume yielding the fractional cumulative surface area in the reservoir as a function of fractional cumulative volume of the reservoir, sorted by increasing matrix block volume. This process was repeated for a wide variety of average fracture spacings. Figure 2 shows this relationship for three arbitrary sets of average fracture spacings. It can be seen that there is little difference between these curves for different fracture spacings. This

relationship can be approximated by the following equation:

$$A_{frac} = V_{frac}^{0.47} . \quad (24)$$

This curve is shown in Fig. 2 without plot symbols.

The characteristic fractional cumulative surface areas for each matrix domain are obtained by substituting the midrange cumulative volume fractions for the matrix domains into Eq. 24. The characteristic fractional cumulative matrix domain surface areas for each of the two domains are then normalized by dividing them by the characteristic fractional area of the reservoir if the reservoir were modeled as having only a single matrix domain, i.e., they are divided by the fractional cumulative area from Eq. 24 at a mid-range fractional cumulative volume fraction of 0.5. This fractional area is 0.72. This gives the normalized fractional cumulative surface area for each domain relative to that of a reservoir with a single matrix domain.

The final step is to relate the normalized fractional cumulative surface areas to the measured average fracture spacings. This is done by multiplying the values of average fracture spacings by the square root of the normalized fractional cumulative surface area for each domain and using those values in Eq. 9. This approach extends the method for a single matrix domain to two matrix domains. The square root is used because it yields the proper adjusted surface area for each domain when two lengths are multiplied to get an area.

Late-Time Period

The fracture spacing data is incorporated into the late-time period models in a different way because the thermal cross flow during this period is not governed by the matrix block surface areas. For this case, a direct relationship was obtained between the matrix block size parameter, R, and the statistical parameters governing the fracture spacing distribution through Monte Carlo simulation. Fracture spacing realizations were obtained for three orthogonal directions assuming different negative exponential fracture spacing distributions in each of the three directions. Each set of three fracture spacings was then ordered such that $L_X < L_Y < L_Z$. These values were then substituted into Eq. 22 to obtain individual matrix block size parameters. The associated matrix block volumes were also determined by multiplying the three fracture spacings. This process was repeated thousands of times to obtain a statistical distribution between the matrix block size parameter and the matrix block volume.

The matrix block size parameters and volumes were then sorted in order of increasing matrix block size parameter and the cumulative volume fraction determined. These values were then curve-fit to a log-normal distribution of the cumulative matrix block volume as a function of increasing matrix block size parameter:

$$P(V_{frac}) = \frac{1}{\sqrt{2\pi}} \int_{-\infty}^{\frac{\ln(R)-\mu_R}{\sigma_R}} \exp\left\{-\frac{u^2}{2}\right\} du \cdot \quad (25)$$

For a negative-exponential fracture spacing distribution, it was found that the log-normal relationship between the matrix block size parameter and volume could be reasonably modeled with the following parameters:

$$\mu_R = 2\ln\left(\frac{1}{\langle L_x\rangle} + \frac{1}{\langle L_y\rangle} + \frac{1}{\langle L_z\rangle}\right) + 1.41 \quad (26)$$

and

$$\sigma_R = 1.45 , \quad (27)$$

where $\langle L_x\rangle$, $\langle L_y\rangle$, and $\langle L_z\rangle$ are the respective average fracture spacings for the three orthogonal fracture sets defining the fracture network. One such data set is shown in Fig. 3.

A dimensionless matrix block size parameter was defined as

$$X_R = \frac{\ln(R) - \mu_R}{\sigma_R} \quad (28)$$

and is plotted in Fig. 4 terms of the cumulative matrix block volume. The matrix block size parameter, R, is determined from the dimensionless matrix block size parameter by inverting Eq. 28:

$$R = \exp\{X_R\sigma_R + \mu_R\} , \quad (29)$$

where μ_R and σ_R are obtained from Eqs. 26 and 27, respectively.

The late-time period model is used by selecting the matrix domain volume fractions and corresponding midrange volume fractions, determining the dimensionless matrix block size parameter from Fig. 4 using the midrange volume fractions (y-axis), calculating the matrix block size parameter from Eq. 29 with the measured average fracture spacings, and then using those parameters in Eq. 23 for the case of a single matrix domain or Eq. 21 for two matrix domains.

COMPARISON ON MODELS

The effect of using fracture spacing information in the models for the area of the thermal zone is demonstrated in this section. The fracture spacing

distribution for the example reservoir are assumed to follow the negative-exponential distribution, with average spacings of 10 m, 20 m, and 100 m in the three orthogonal directions, respectively. The other properties are given in Table 1.

Early-Time, One Matrix Domain

The values of L_x, L_y, and L_z to be used in Eq. 9 are the average fracture spacings, 10 m, 20 m, and 100 m, respectively. For this case, χ_1 =1 and χ_2 =0. The resulting area of the thermal zone is plotted in Fig. 5 as a function of time.

Early-Time, Two Matrix Domains

It will be assumed that the two matrix domains have equal volume fractions. The midrange volume fractions are 0.25 and 0.75, respectively for the two domains. The corresponding area fractions from Eq. 24 are 0.52 and 0.87, for the respective domains. The normalized area fractions after dividing by 0.72 are 0.72 and 1.21, respectively. The average fracture spacings for the two domains are then obtained by multiplying the measured average fracture spacing by the square root of the normalized area fraction. The values of L_x, L_y, and L_z to be used in Eq. 9 are then 8.5 m, 17.0 m, and 85 m for the first domain and 11 m, 22 m, and 110 m for the second domain. The resulting area of the thermal zone is plotted in Fig. 5 as a function of time.

Late-Time, One Matrix Domains

For the assumed fracture spacing distribution, the dimensionless matrix block size parameter is determined from Fig. 4 at the midrange volume fraction of 0.50. This yields a dimensionless matrix block size parameter of 1. The statistical values for the mean and standard deviation of the logarithm of the fracture spacings from Eqs. 26 and 27 are -2.26 and 1.45, respectively. The resulting matrix block size parameter is given by Eq. 29 as 0.44 m^{-2}. This matrix block size parameter was then used in Eq. 23. The resulting area of the thermal zone is plotted in Fig. 5 as a function of time.

If all matrix blocks were identical and had the same dimensions as the average fracture spacing, the value of the matrix size parameter can be determined directly from Eq. 22. However, uniform matrix blocks are not consistent with the assumption of a negative-exponential fracture spacing distribution.

Late-Time, Two Matrix Domains

It will be assumed that the two matrix domains have equal volume fractions. The midrange volume fractions are 0.25 and 0.75, respectively for the two domains. The corresponding logarithms of the dimensionless matrix block size parameter from Fig. 1 are -0.67 and 0.67, for the respective domains, yielding dimensionless matrix block size parameters of 0.512 and 1.95, for the two domains, respectively. The values for the mean and standard deviation of the logarithm of the fracture spacings given by Eqs. 26 and 27 are -2.26 and 1.45, respectively. The resulting matrix block size parameters are given by Eq. 29 as 0.22 m^{-2} and 1.76 m^{-2} for the two domains, respectively. These matrix block size parameters are then used in Eq. 21. The resulting area of the thermal zone is plotted in Fig. 5 as a function of time.

Discussion

The four models demonstrated in this section are shown in Fig. 5. This figure shows that the difference between the double-porosity and triple-porosity models, i.e., one or two matrix domains, is minor. Within the typical accuracy of most fracture spacing data, the additional complication of using models having multiple matrix domains is probably not justified.

The approximate time when the early-time period ends for time for this example (given by Eq. 8) is about 40 days. Before this time, the early-time period models are believed to be most accurate, while after this time, the late-time period models are believed to be most accurate.

CONCLUSIONS

New models have been presented for estimating the size of the thermal zone in a geothermal reservoir following reinjection. These models utilize thermal conduction models previously presented (Reis, 2000). Models have been presented for both the early-time period in which conduction fronts in the matrix blocks from opposite sides have not yet merged at the matrix center and for the late-time period in which the conduction fronts have merged. In both cases, models have been presented for a traditional double-porosity reservoir having one matrix domain and for a triple-porosity reservoir having two matrix domains. The difference between the double- and triple-porosity models is minor. For each model, a method for incorporating measured statistical fracture spacing information was also presented.

ACKNOWLEDGEMENT

This work was funded by the U.S. Department of Energy, Idaho Operations Office, under grant DE-FG07-99ID13746

REFERENCES

Baecher, G. B., Lanney, N. A., and Einstein, H. H., "Statistical Description of Rock Properties and Sampling," Proc. 18th US Symp. Rock Mechanics, pp. 501-508, 1977.

Bodvarsson, G. S. and Tsang, C. F., "Injection and Thermal Breakthrough in Fractured Geothermal Reservoirs," J. Geophysical Res., Vol. 87, No. B2, pp. 1031-1048, Feb. 10, 1982.

Call, R. D., Savely, J. P., and Nicholas, D. E., "Estimation of Joint Set Characteristics from Surface Mapping Data," Proc. 17th US Symp. on Rock Mechanics, Salt Lake City, Utah, Vol. 2b2, 1976.

Closmann, P. J., "Steam Zone Growth During Multiple-Layer Steam Injection," Soc. Pet. Eng. J., pp. 1-10, March, 1967.

Einstein, H. H., Baecher, G. B., and Veneziano, D., "Risk Analysis for Rock Slopes in Open Pit Mines," Part I and Final Technical Report to US Bureau of Mines, Nov. 1979.

Einstein, H. H. and Baecher, G. B., "Probabilistic and Statistical Methods in Engineering Geology: Specific Methods and Examples, Part I: Exploration," Rock Mechanics and Rock Engineering, Vol. 16, pp. 39-72, 1983.

Gringarten, A. C., Witherspoon, P. A., and Ohnishi, Y., "Theory of Heat Extraction from Fractured Hot Dry Rock," J. Geophysical Res., Vol. 80, No. 8, pp. 1120-1124, March 10, 1975.

Hearn, C. L., "Effect of Latent Heat Content of Injected Steam in a Steam Drive," J. Pet. Tech., pp. 374-375, April 1969.

Lauwerier, H. A., "The Transport of Heat in an Oil Layer Caused by the Injection of Hot Fluid," Appl. Sci. Res. A, Vol. 5, pp. 145-150, 1955.

Mahtab, M. A., Bolstad, D. D., and Kendorski, F. S., "Analysis of the Geometry of Fractures in San Manual Copper Mine, Arizona," U. S. Department of the Interior, Bureau of Mines, Report of Investigations 7715, 1973.

Marx, J. W. and Langenheim, R. H., "Reservoir Heating by Hot Fluid Injection," Trans. AIME, Vol. 216, pp. 312-315, 1959.

Priest, S. D. and Hudson, J. A., "Discontinuity Spacing in Rock," Int. J. Rock Mech. & Min. Sci., Vol. 13, pp. 135-148, 1976.

Reis, J. C., "New Analytical Models for Multi-Dimensional Thermal Conduction in Fractured Geothermal Reservoirs," presented at the 25th Stanford Workshop on Geothermal Reservoir Engineering, January 2000.

Satman, A., "Solutions of Heat- and Fluid-Flow Problems in Naturally Fractured Reservoirs: Part 2 - Fluid Flow Problems," SPE Production Engineering, pp. 467-473, Nov. 1988.

Sen, Z. and Eissa, E. A., "Rock Quality Charts for Log-Normally Distributed Block Sizes," Int. J. Rock Mech. Min. Sci. and Geomech. Abstr., Vol. 29, pp. 1-12, 1992.

Wallis, P. F. and King, M. S., "Discontinuity Spacings in a Crystalline Rock," Int. J. Rock Mech., Min. Sci. Geomech. Abstr., Vol. 17, pp. 63-66, 1980.

Table 1 Example Reservoir Data

L	10 m
h_{inj}	1.0×10^6 J/s
H	100 m
k_m	2.8W/m/K
ρ_M	2630 kg/m^3

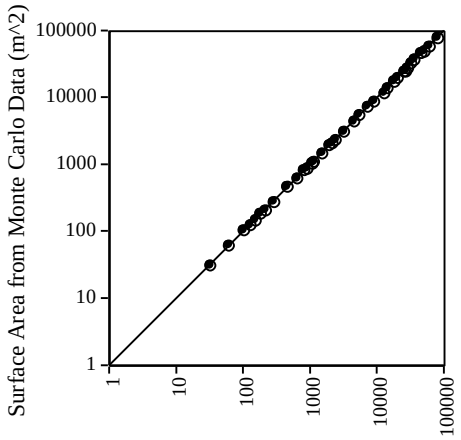

c_m	800 J/kg/K
ΔT	200 K

Figure 1. Comparison of Average Matrix Block Surface Areas

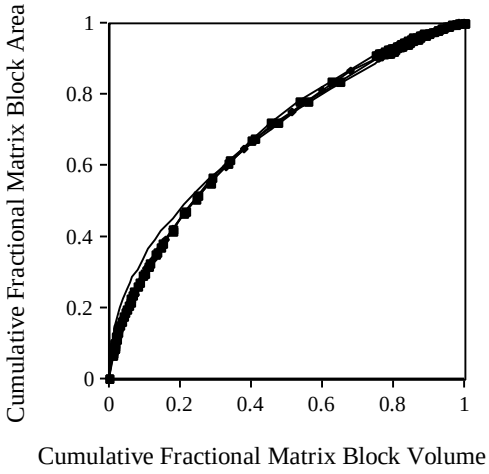

Figure 2. Relationship Between Fractional Surface Area and Fractional Volume

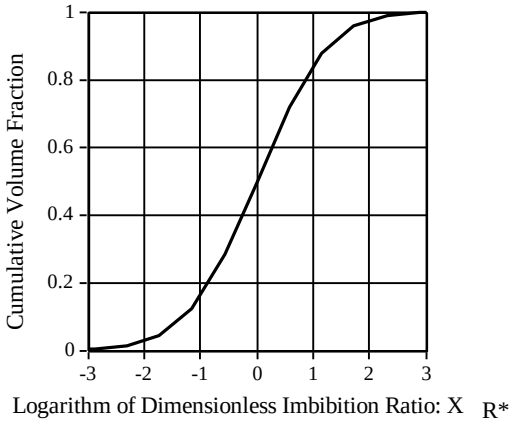

Figure 3. Log-Normal Model for Matrix Block Size Parameter

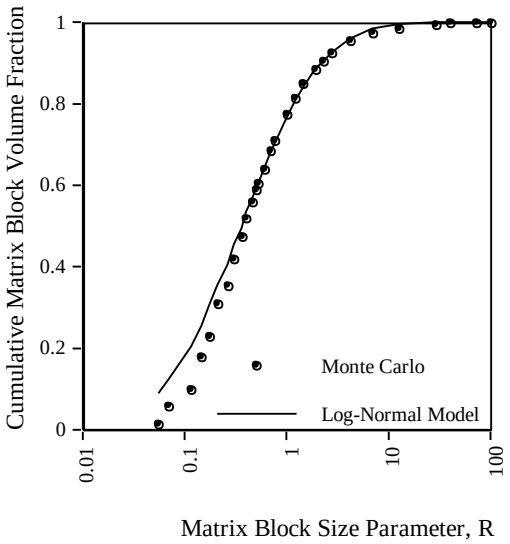

Figure 4. Dimensionless Relationship Between Matrix Block Size Parameter and Matrix Block Volume Fraction

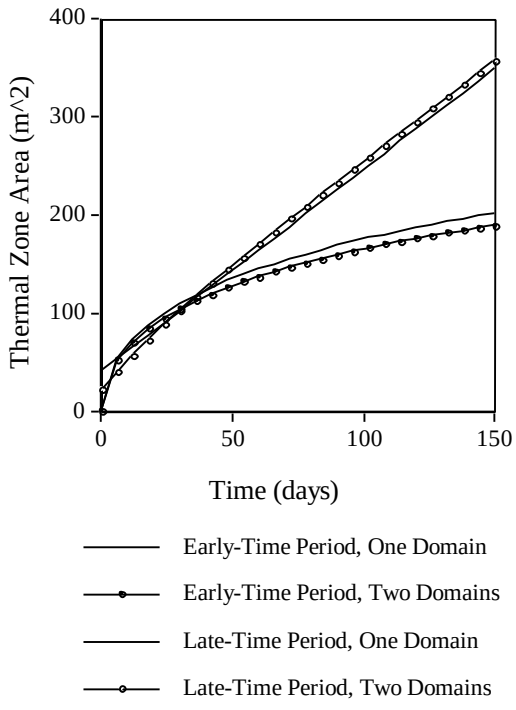

Figure 5. Comparison of Models